**Article:**
Nar, K., Majewski, C. and Lewis, R. (2023) Evaluating the effect of solid lubricant inclusion on the friction and wear properties of Laser Sintered Polyamide-12 components. Wear, 522. 204873. ISSN: 0043-1648

https://doi.org/10.1016/j.wear.2023.204873

Wear 522 (2023) 204873

Contents lists available at ScienceDirect

Wear

journal homepage: www.elsevier.com/locate/wear

# Evaluating the effect of solid lubricant inclusion on the friction and wear properties of Laser Sintered Polyamide-12 components

Kieran Nar *, Candice Majewski, Roger Lewis

*Department of Mechanical Engineering, University of Sheffield, Sheffield, UK*

ARTICLE INFO

*Keywords:*
Additive Manufacturing
Laser Sintering
Tribology
Solid lubricants
Polymer matrix composites
Friction
Wear

ABSTRACT

The processing of Polyamide-12 (PA12) by Laser Sintering is one of the most well-established Additive Manufacturing (AM) processes for producing functional components for end-use applications. However, its further adoption within industry remains hindered by an incomplete understanding of resultant part quality and the impact this has on component wear. The scope of this research was to investigate the dry sliding behaviour of Laser Sintered Polyamide-12, as well as evaluate whether the inclusion of solid lubricant fillers effect the friction and wear properties of parts produced. Polytetrafluoroethylene (PTFE), Graphite and Molybdenum disulphide ($MoS_2$) were added to Polyamide-12 powder in 1 : 100 mass ratios, respectively, to create three different polymeric composites. Mechanical blending and Laser Sintering then ensued; the latter was performed using identical processing parameters throughout. Tribological performance was evaluated by ball-on-flat uni-directional wear testing. Tensile testing was also carried out to help elucidate what wear mechanisms were active during sliding, as well as identify whether solid lubricant inclusion impacted mechanical performance. Results showed that in all instances solid lubricant inclusion significantly influenced the friction and wear properties of resultant composites, without compromising their mechanical performance when compared with neat-PA12. More specifically, it was demonstrated that the individual additions of PTFE and $MoS_2$ could reduce the coefficient of friction and specific wear rate of Laser Sintered PA12 components by as much as 50% and 78%, respectively.

## 1. Introduction

Additive Manufacturing (AM) is the term used for a group of manufacturing technologies which produce parts in a layer-by-layer fashion directly from a digital file. Despite still being an emerging technology (the first commercial system was launched ~ 35 years ago) these techniques have moved beyond their originally intended use for prototyping, and are becoming increasingly adopted within industry for manufacturing functional components for end-use applications [1]. Currently, approximately 33.7% of all AM parts produced are intended for end-use [2]. A multitude of AM techniques are commercially available [3], with differences arising based on what form and types of feedstock material can be processed, as well as the exact processing method used to do so [4]. ASTM International [5] have defined the following structure to group these AM technologies into seven distinct categories: Binder Jetting, Directed Energy Deposition, Material Extrusion, Material Jetting, Sheet Lamination, Vat Photopolymerisation and Powder Bed Fusion. The focus of the research presented here is on Powder Bed Fusion, and more specifically on the polymer Laser Sintering process.

### 1.1. Polymer Laser Sintering

Polymer Laser Sintering (LS) is a subset of Powder Bed Fusion, whereby material is selectively melted layer-by-layer using a laser (or multiple lasers) to consolidate powder into parts [6]. A schematic of the general LS build process can be seen in Fig. 1.

### 1.2. Polyamide-12

Polymer powders currently constitute the largest segment within the AM materials market [2]. The most established LS polymers are variations of Polyamide (PA) [8], with PA12 comprising of approximately 90% of the LS materials market [9]. Polyamide-12 is a semi-crystalline polymer popular for LS due to its inherent processability; owing to its wide sintering window [10], and relatively good recyclability [11].

* Corresponding author.
*E-mail address:* knar1@sheffield.ac.uk (K. Nar).

https://doi.org/10.1016/j.wear.2023.204873
Received 2 October 2022; Received in revised form 2 February 2023; Accepted 5 February 2023
Available online 29 March 2023

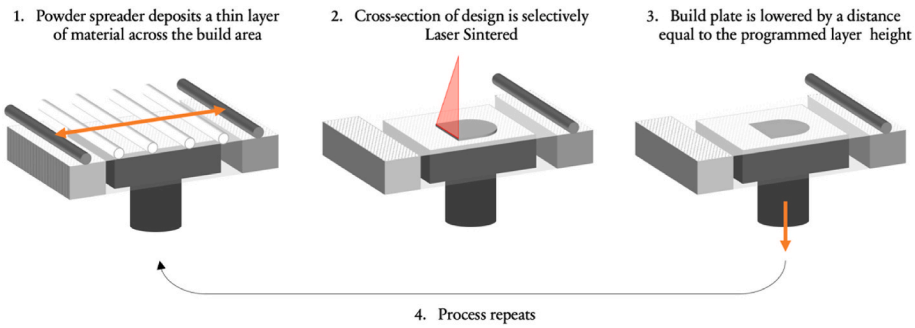


**Fig. 1.** A schematic of the polymer Laser Sintering build process, adapted from Kruth et al. [7].

Other advantageous attributes include high toughness [12], good specific strength [13] and excellent resistance to abrasion, creep and fatigue [12–14] relative to other polymers. However, despite a reasonably good body of existing literature relating to static mechanical properties, limited research is available that pertains to the performance of LS PA12 components when subject to dynamic contact.

### 1.3. Polyamide-12 composites

In recent years, the inclusion of inorganic fillers within PA12 matrices has been explored as a way of introducing additional functionality to LS polymer components to improve their suitability for end-use applications [9,15]. A selection of fillers as well as their resultant benefits is shown in Table 1.

Several additional factors must be considered to ensure filler reinforced polymeric composites are processable by LS, and that they attain their required functionality. These include: the specific filler reinforcement material, size [9], morphology [16], interfacial adhesion [17,18] and percentage weight addition (%wt) [19], as well as the preparation method performed to combine material constituents [20].

As can be seen in Table 1, Bai et al. [25] improved the tribological performance of LS PA12 samples by including 1 %wt of Molybdenum disulphide ($MoS_2$). The addition of this solid lubricant reduced coefficient of friction (COF) and wear rate by 56.7% and 41.7%, respectively, during linear reciprocating ball-on-flat wear testing. The research presented in this paper will investigate a broader range of solid lubricants, in order to establish their suitability for use in Laser Sintering and whether they also induce a lubricating response.

### 1.4. Solid lubricants

Solid lubrication is becoming integral within polymer tribosystems where friction and wear are critical issues [30,31]. Bart et al. [32] highlighted that many materials qualify as solid lubricants but their intrinsic ability to reduce friction and wear arise by different mechanisms.

Structural solid lubricants have layered lattice structures and thus conform to the lamellar mechanism of lubrication, whereby weak bond strengths between layers allow for them to shear easily when subject to loads parallel to their planar directions [33]. Moreover, transfer film formation is characteristic of structural solid lubricant inclusion, which typically modifies a contact such that dry sliding instead occurs between the substrate and transferred alike material adhered on the original counterface [34]. Mariani [33] identified Graphite and $MoS_2$ to be the most well-established structural solid lubricants. Both have laminar crystal lattice structures that comprise of strong covalently bonded hexagonal planes separated by comparatively weaker Van der Waals forces [35]. Ben Difallah et al. [36] evaluated the mechanical and tribological performance of compression moulded Acrylonitrile Butadiene Styrene (ABS) composites containing Graphite in varying weight percentages ranging from 0 %wt – 7.5 %wt. They found the addition of Graphite, independent of %wt inclusion, improved both coefficient of friction and wear rate. However, this was at the detriment of Young's modulus (YM), Ultimate Tensile Strength (UTS) and Elongation at Break (EaB) which were all inferior to pure ABS samples.

Polytetrafluoroethylene (PTFE) is another well recognised solid lubricant. However, unlike Graphite and $MoS_2$, PTFE is an organic polymer that is lubricious due to its high softening point [37] and smooth macro molecular polymer chain profiles, which orient to facilitate slip [33]. Despite its exceptional efficacy as a low friction additive, PTFE is very susceptible to wear [38] and therefore rarely used for sliding applications in its neat form. Li et al. [39] found that PTFE inclusion within glass reinforced PA6 injection moulded specimens could reduce COF and wear rate by 29.9% and 28.9%, respectively, during linear reciprocating ball-on-flat wear testing. Moreover, these resultant reductions in friction and wear were correlated with PTFE loading ratios, which ranged from 0 %wt – 20 %wt.

The work presented here investigates whether the inclusion of solid lubricants within PA12 matrices can reduce the friction and wear properties of resultant Laser Sintered components, without compromising their mechanical performance.

**Table 1**
A selection of different filler materials and the new or enhanced properties they can induce in Laser Sintered PA12 matrices.

| Filler material | Research details | Part properties that have been improved and/or introduced |
|---|---|---|
| Glass beads | Majewski et al. [21] | Young's Modulus |
| Carbon fibres | Liu et al. [22] | Ultimate Tensile Strength |
| Aluminium | Mazzoli et al. [23] | Rigidity, post-processability, heat deflection |
| Potassium titaniumwhiskers | Yang et al. [24] | Ultimate Tensile Strength, flexural strength, flexural modulus |
| Molybdenum disulphide | Bai et al. [25] | Wear rate, coefficient of friction |
| Zinc borate | Batistella et al. [26] | Flame retardancy |
| Silver phosphate glass | Turner et al. [27] | Antimicrobial efficacy |
| Nanosilica | Chunze et al. [28] | Thermal stability, Ultimate Tensile Strength, Young's Modulus, impact strength |
| Carbon nanotubes | Bai et al. [29] | Flexural modulus, flexural strength, impact strength, Young's Modulus, Ultimate Tensile Strength |

## 2. Material and methods

### 2.1. Materials

Commercial grade Polyamide-12, specifically PA2200 supplied by EOS GmbH, was blended with the solid lubricants discussed in Section 1.4 to create three different polymeric composites, hereinafter referred to as PTFE-PA12, Graphite-PA12 and $MoS_2$-PA12.

The PA12 matrices comprised of sieved virgin material which had an average particle size of 56μm [40]. Solid lubricant particle sizes, as quoted by the supplier, are listed in Table 2. These were incorporated into each PA12 matrix in mass ratios of 1 : 100 (solid lubricant : PA12). More explicitly, each batch of polymeric composite powder had a total weight of 3.03kg, which comprised of 30g of solid lubricant added to 3kg of PA12 powder. This solid lubricant loading ratio and particle size range was chosen to minimise agglomeration during dry mixing so that a uniform dispersion could be attained [9].

Each polymeric composite was blended by rotary tumbling at a speed of 12.5rpm for 60 minutes upon filler inclusion, and for a further 60 minutes prior to loading each polymeric composite into the Laser Sintering machine.

Resultant samples were evaluated with respect to neat-PA12 control specimens which were also Laser Sintered from the same batch of sieved virgin PA2200 material.

### 2.2. Sample preparation

The Laser Sintering build process was performed using an EOS Formiga P100 system, programmed with previously determined processing parameters optimised for PA2200 as detailed in Table 3. To ensure the resultant effect of each solid lubricant was evaluated systematically, individual composite LS processing parameters were kept constant in this study.

For each material, samples produced included multiple disk specimens for friction and wear testing with major dimensions equal to 80mm × 5mm (diameter x thickness), as well as five ASTM D638 Type 1 specimens for tensile testing. Samples were arranged with at least 5mm margins in every direction to minimise any thermal interactions that may have occurred between neighbouring parts during building.

Once the Laser Sintering build process was complete and the parts fully cooled to ambient temperature, compressed air was used to remove loose powder particles from the surfaces of PA12, Graphite-PA12 and $MoS_2$-PA12 samples. PTFE-PA12 samples were observed to have 'harder' powder cakes so additional glass bead blasting was required to break these samples out from their surrounding powder.

### 2.3. Characterisation

#### 2.3.1. Filler dispersion

A Hitachi TM3030 desktop Scanning Electron Microscope (SEM) was used to identify solid lubricant dispersions within each PA12 matrix and whether any agglomeration occurred as a result of rotary blending. Mixed secondary electron and back scattering images were captured using a 15kV accelerating voltage configured with large current mode.

**Table 2**
Solid lubricant particle sizes, as quoted by the supplier.

| Solid lubricant | Size (μm) | Supplier |
|---|---|---|
| Graphite | Particle size distribution (PSD) = 5 – 10 | Nanografi |
| Molybdenum disulfide | Average particle size (D50) = 4.5 | Lower Friction |
| Polytetrafluoroethylene | Average particle size (D50) = 3 | Lower Friction |

**Table 3**
Laser Sintering build parameters [18] used within this study.

| Processing parameter | Value |
|---|---|
| Laser power (W) | 21 |
| Beam spacing (mm) | 0.25 |
| Scan speed ((mm)$s^{-1}$) | 2500 |
| Bed temperature ($^oC$) | 170 |
| Scan count | 1 |
| Layer thickness (mm) | 0.1 |

#### 2.3.2. Surface analysis

Focus Variation (FV) microscopy was used to evaluate the surface topographies and wear scars of polymeric specimens, as well as any material transfer that occurred to the counterface pin surfaces post testing; the former was characterised by Root Mean Square roughness ($S_q$) and Skewness ($S_{sk}$). ISO 25178–2 [41] defines $S_q$ as the square root of the mean square of the ordinate values of a scale-limited surface, and $S_{sk}$ as the quotient of the mean cube value of the ordinate values of a scale-limited surface and the cube of $S_q$. Alternatively, $S_q$ and $S_{sk}$ describe the magnitude of vertical height deviations and symmetry of peaks and valleys about a surfaces mean plane, respectively. These values were measured at three different locations on three different specimens for each material.

All areal surface analysis was performed using an Alicona InfiniteFocusSL system equipped with a ×5AV objective lens, which captured evaluation areas 3.665mm × 3.665mm in size with a vertical resolution of 550 nm. Areal roughness values were computed without spatial filtering, in concurrence with works by Petzold et al. [42], Newton et al. [43] and Zhu et al. [44]. Though, when extracting 2D wear scar profiles from 3D areal surface topography scans, a cut-off length of 0.8mm was applied in accordance with ISO 13565–1 [45].

#### 2.3.2. Tensile testing

A Tinius Olsen H5KS tensometer with a H500L laser extensometer was used to measure the tensile properties of resultant specimens, specifically Young's Modulus, Ultimate Tensile Strength and Elongation at Break, in accordance with ASTM D638-14 [46]. Tensile loads were applied perpendicular to the build direction at a speed of 5(mm)$min^{-1}$ and cross-sectional areas were calculated from mean width and thickness measurements taken at three different locations along the gauge length of each specimen.

#### 2.3.4. Friction and wear testing

Ball-on-flat, rotating, uni-directional, pin-on-disk tests were performed under dry sliding conditions using a Bruker Universal Mechanical Tester (UMT) TriboLab configured with a rotary module and 50N

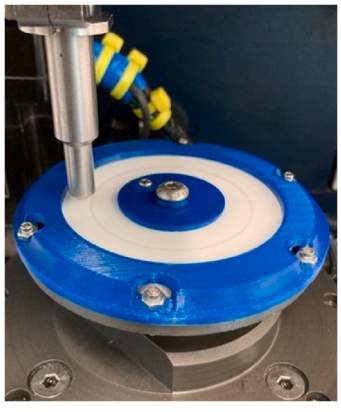

**Fig. 2.** The ball-on-flat, pin-on-disk wear test configuration used within this study.

load cell accurate to ±2.5mN. A stainless steel ball, 6.35mm (1/4 in) in diameter, comprised the contacting proportion of the pin counterface and was loaded against the top surface of each Laser Sintered disk sample. The polymeric Laser Sintered disks were attached to the rotary module using a central screw to ensure concentricity, as well as being fastened at the edges to prevent slipping and to best achieve flatness relative to the rotary module, respectively. This can be seen in Fig. 2.

Tests were conducted under a tangential velocity of $0.35 ms^{-1}$ over a length of 1000m, and at low and high applied normal loads of 10N and 30N, respectively. Corresponding low and high Hertzian contact pressures between the steel pin counterface and neat-PA12, PTFE-PA12, Graphite-PA12 and $MoS_2$-PA12 disks were calculated to be 55.4MPa and 79.9MPa; 54.4MPa and 78.4MPa; 62.4MPa and 90.1MPa; and 62.1MPa and 89.6MPa, respectively. COF data was recorded at a sampling rate of 1Hz and tests were repeated three times for each polymeric disk material so that mean values could be obtained.

Post-testing, resultant wear scar geometries were analysed by FV microscopy so that wear volumes ($V$) could be calculated using Eq. (1), as detailed in ASTM G99 [47],

$$V = 2\pi R\left[r^2 \sin^{-1}\left(\frac{d}{2r}\right) - \frac{d}{2}\sqrt{r^2 - \frac{d^2}{4}}\right]\left[mm^3\right] \quad (1)$$

where $R$ is the wear track radius (mm), $r$ is the pin end radius (3.175 mm), and $d$ is the resultant wear track width (mm) - which in this study was measured at four different locations. Furthermore, specific wear rates for each material were calculated using Eq. (2) below,

$$W_s = \frac{V}{F_N \times L}\left[mm^3 / Nm\right] \quad (2)$$

where $F_N$ is the applied normal load (N) and $L$ is sliding distance (m).

## 3. Results and discussion

### 3.1. Laser Sintering

All samples were successfully Laser Sintered using the processing parameters listed in Table 3. Distinct smaller particles with sizes and morphologies that correspond to the solid lubricants used within this study can be seen in the SEM image presented in Fig. 3. These particles are well dispersed within their respective matrices and no qualitive evidence of agglomeration (which might have led to the impediment of powder flow) was observed during building.

Ultimately, solid lubricant particle size distributions, within the range of 3μm – 10μm, blended by dry mixing were found to be suitable for producing homogenous composite PA12 powders with good flow properties.

During processing, Graphite-PA12 and $MoS_2$-PA12 samples experienced curl localised at the perimeters of each disk specimen. Practically, this would render many parts produced as being unsuitable for end-use applications and in this study prevented repeat wear tests of $MoS_2$-PA12 samples from being carried out at 30N. This phenomenon is intrinsic to polymer Laser Sintering and typically occurs when there is too extreme a temperature differential between the bulk and upper surface of the part during building, whereby the latter will typically be lower in temperature, particularly at the edges of the part, due to being convectively cooled every time a new powder layer is deposited. This thermal gradient induces residual stresses within each part, resulting in differential shrinkage at their edges where the temperature difference will have been the greatest. The disk specimens in this study also had large cross-sections relative to the build area, which will have led to significant in situ cooling during the scanning of each layer [48]. In addition, $MoS_2$ and Graphite both have thermal conductivities an order of magnitude greater than PA12 at room temperature [32,49–51], thus the temperature differentials within Graphite-PA12 and $MoS_2$-PA12 parts are likely to have been exacerbated due to more heat being in their

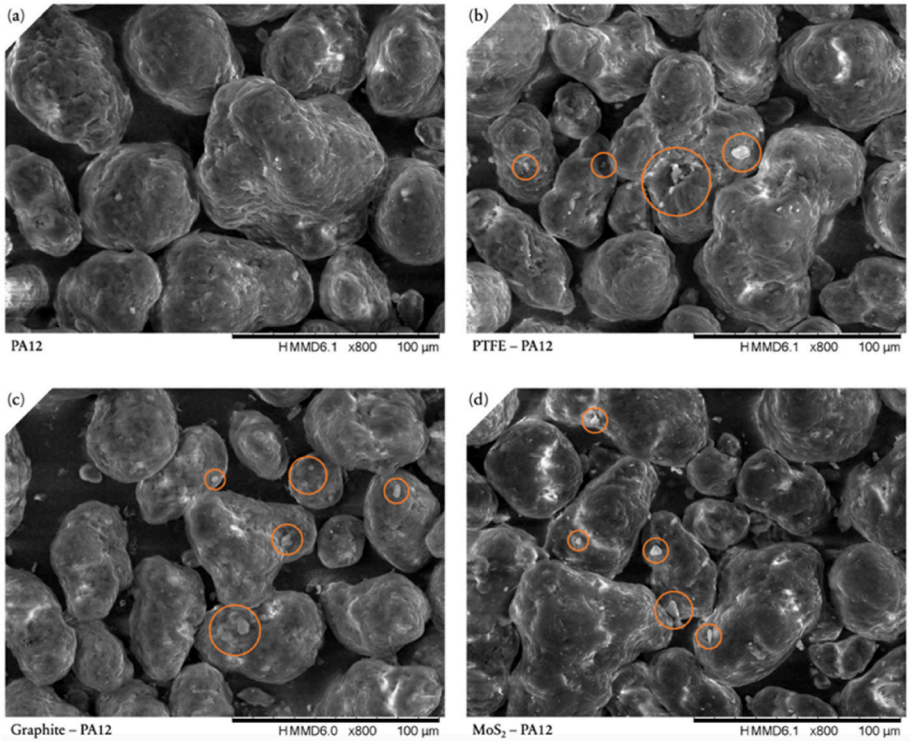


**Fig. 3.** SEM images of each feedstock material Laser Sintered in this study, which included (a) PA12 virgin powder, as well as (b) PTFE, (c) Graphite and (d) $MoS_2$ filled PA12 composite powders. Solid lubricant particulates have been highlighted in orange. (For interpretation of the references to colour in this figure legend, the reader is referred to the Web version of this article.)

powder beds during building. To minimise curl, part bed temperatures should be increased nearer to each composite powder's glaze temperature. Auxiliary to this, Goodridge et al. [52] demonstrated double scanning each layer assisted in preventing curl. As previously discussed in Section 2.2 individual material processing parameters were not optimised in order to systematically characterise any effects solid lubricant inclusion had on the friction and wear properties of composite parts produced relative to neat-PA12.

Also, PTFE-PA12 samples required additional glass media blasting to remove their significantly harder powder cakes, the occurrence of which Bourell et al. [53] attributed to part bed temperatures being too high.

### 3.2. Surface topographies

Fig. 4 shows the effect of individual PTFE, Graphite and $MoS_2$ inclusions on the resultant top surface topographies of Laser Sintered PA12 samples. More specifically, the addition of these solid lubricants increased vertical height deviations by 2.24μm, 2.08μm and 1.91μm, relative to neat-PA12, respectively. Despite this, all measured top surface $S_q$ values were in good agreement with LS polymer roughness studies conducted by Petzold et al. [42] and Vetterli et al. [54]. Furthermore, it can be seen in Fig. 4b that all sample top surfaces were measured to have positive Skewness values and were therefore all asperity peak dominated. However, resultant PTFE-PA12 sample top surfaces were notably more Gaussian, which suggests the inclusion of PTFE impeded the mechanism of top surface modification through powder particle adhesion [55].

### 3.3. Tensile properties

For each material, resultant stress-strain curves and their mean tensile properties are shown in Fig. 5 and Table 4, respectively. It can be seen the mechanical performance of PTFE-PA12, Graphite-PA12 and $MoS_2$-PA12 composites were reasonably comparable with neat-PA12, which suggests the inclusion of these solid lubricants did not promote crack initiation leading to premature failure. Moreover, the addition of $MoS_2$ increased resultant part stiffness, strength and ductility relative to neat-PA12 samples. Similar findings were made by Bai et al. [25], who demonstrated impact strength could be increased by 11.4% as a result of $MoS_2$ reinforcement when optimised Laser Sintering processing parameters were employed.

The addition of Graphite reduced resultant part ductility, but increased Young's Modulus and UTS relative to neat-PA12 samples. As previously mentioned, both Graphite and $MoS_2$ have thermal conductivities an order of magnitude greater than PA12, therefore more heat will have been in each materials powder bed during processing and as a result greater part densification is likely to have ensued [56]. Furthermore, Kigure et al. [57] found that Laser Sintering PA12 at higher powder bed temperatures produced parts with increased crystallinities, strength and stiffness. Contrastingly, the addition of PTFE reduced part stiffness and strength, but increased ductility by 77.8% relative to neat-PA12 samples. In virgin form PTFE has a greater Elongation at Break compared to PA12 [58,59], so its inclusion within the latter will have been the reason PTFE-PA12 was more ductile than neat-PA12.

Ultimately solid lubricant inclusion in accordance with the material preparation method outlined in Section 2.1 did not compromise resultant composite part properties relative to Laser Sintered neat-PA12.

### 3.4. Friction

Raw coefficient of friction data for each material and loading condition is shown in Fig. 6. Mean COF values, computed over the entire 1000m test distance, are listed in Table 5 and percentage comparisons in tribological performance between Laser Sintered neat-PA12 and each solid lubricant filled polymeric composite can be seen in Fig. 8.

PTFE-PA12 was the only solid lubricant filled composite that demonstrated a major change in frictional response relative to neat-PA12. During 10N wear testing a 37.1% mean reduction in COF was achieved as shown in Fig. 8a. Furthermore, under this low load test condition PTFE-PA12 facilitated the smoothest sliding, as indicated by resultant samples having the least variation in raw COF data relative to every other material tested. A transfer film was observed on each corresponding counterface after 10N wear testing of PTFE-PA12 samples, as can be seen in Fig. 9b. Therefore, a proportion of dry sliding will have instead occurred between alike self-lubricating polymer material rather than entirely with the metallic counterface.

At the higher load test condition of 30N, friction was initially reduced by an even greater magnitude. From 0m – 600m the inclusion of PTFE decreased mean COF to 0.128, which was a 50.1% reduction relative to neat-PA12. Smoother sliding, given by reduced variance in raw COF data, can also be seen in Fig. 6b. However, at approximately 600m PTFE-PA12's lubricating response broke down. This phenomenon was unique to the 30 N loading condition and occurred at a similar point in every repeat test as shown in Fig. 7. In all instances COF sharply increased, doubling within the following 200m, and fluctuated irregularly for the remaining duration of each 1000 m test. The consistency in which PTFE-PA12's lubricating response broke down, both in terms of applied load and moment of occurrence, is indicative of a frictional heating related failure. It is likely resultant thermal softening will have led to the steel counterface further indenting the PTFE-PA12 surface, thus greater ploughing will have ensued and as a result friction will have increased. Furthermore, it can be seen in Fig. 9b that after higher load testing significantly less PTFE-PA12 material adhered to the steel counterface surface. A transfer film was still present within the contact area; however, it was comparatively discontinuous and covered a considerably reduced area fraction relative to the transfer film observed after 10N testing.

In addition, it can also be seen in Fig. 9 that no transfer film was

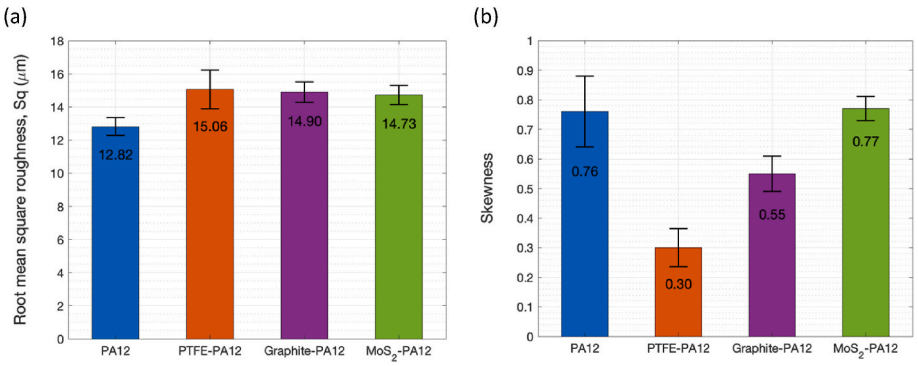


**Fig. 4.** Average top surface topography roughness data describing the (a) magnitude of vertical height deviations and (b) symmetry about each measured surfaces mean plane.

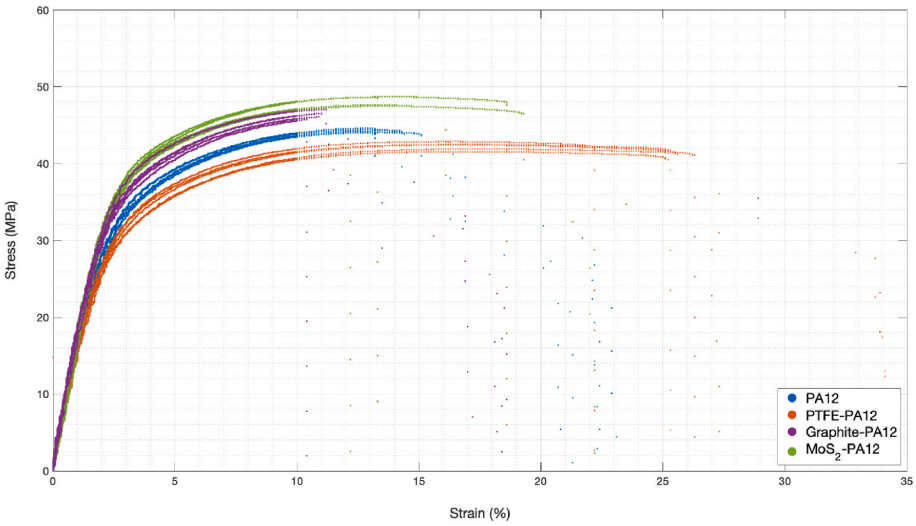


**Fig. 5.** Tensile curves of all specimens evaluated, including repeat tests for each material.

**Table 4**
Mean resultant tensile properties, as well as their corresponding standard deviation values.

| Material | Youngs Modulus (MPa) | Ultimate Tensile Strength (MPa) | Elongation at Break (%) |
|---|---|---|---|
| PA12 | 1464 (±66) | 44.3 (± 0.2) | 14.0 (± 0.8) |
| PTFE-PA12 | 1422 (±79) | 42.2 (± 0.5) | 24.9 (± 1.6) |
| Graphite-PA12 | 1754 (±246) | 46.3 (± 0.5) | 10.8 (± 0.3) |
| $MoS_2$-PA12 | 1740 (±135) | 48.0 (± 0.6) | 15.5 (± 3.3) |

present on each corresponding counterface pin surface after sliding against PA12, Graphite-PA12 and $MoS_2$-PA12 samples independent of load. The lack of lubricating transfer film provides an explanation as to why Graphite-PA12 and $MoS_2$-PA12 induced relatively minor friction lowering responses compared to PTFE-PA12. Moreover, Graphite inclusion reduced COF by 5.2% and 5.7% relative to neat-PA12 under 10N and 30N testing conditions, respectively. It is expected that increasing the percentage weight addition of Graphite would further facilitate sliding, as demonstrated by Ben Difallah et al. [36] and Sathees Kumar et al. [60]. However, this would also prompt processability issues relating to powder flowability and melting and crystallisation behaviours.

As can be seen in Fig. 8a there was negligible difference between the mean COF of $MoS_2$-PA12 and neat-PA12. However, at the higher load test condition of 30N the inclusion of $MoS_2$ did significantly reduce the variance in raw COF data, relative to lower load sliding. Moreover, Mariani [33] identified the lubrication performance of $MoS_2$ to be most effective in higher load applications, where contact pressures are typically orders of magnitude greater than those incurred in this study. Therefore, insufficient applied normal loads are likely to have prevented

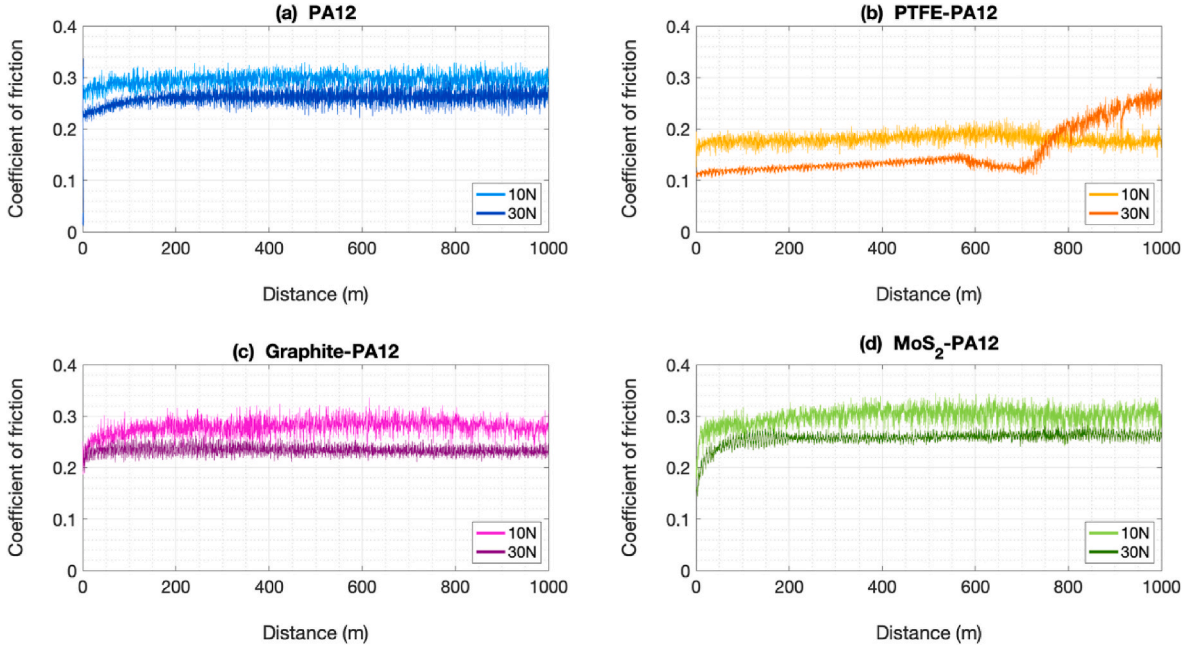


**Fig. 6.** Raw coefficient of friction data for each material examined by ball-on-flat, uni-directional, pin-on-disk testing at 0.35ms$^{-1}$ for 1000m and applied loads of 10N and 30N. Repeat tests were carried out which show similar COF responses for each material and loading condition. Therefore, to best facilitate readability only single COF traces have been included above.

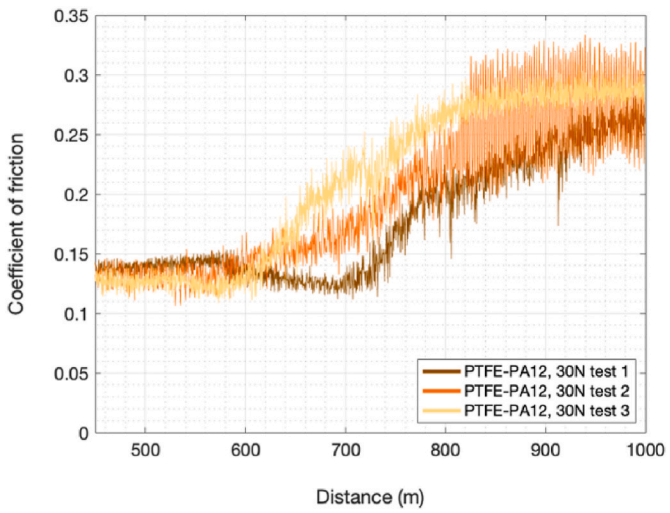


**Fig. 7.** Lubrication breakdown of PTFE-PA12 samples during higher load 30N wear testing.

$MoS_2$ enriched transfer films from forming in this study.

### 3.4. Wear

As previously discussed in Section 2.3.4, wear was characterised volumetrically to compute specific wear rates for each material. These values are detailed in Table 5 and are in good agreement with data collected by Bai et al. [25] and Guo et al. [61]. An inverse trend between friction and wear was observed when comparing the tribological performance of solid lubricant reinforced PA12 composites, independent of load. PTFE-PA12 experienced the most wear, despite sliding with the least resistance, whereas Graphite-PA12 and $MoS_2$-PA12 had the smallest mean specific wear rates, even though they incurred the greatest friction. Furthermore, wear resistance was also correlated to resultant part strength and stiffness. More specifically, materials with greater Ultimate Tensile Strength's and Young's Moduli experienced smaller amounts of wear, and vice versa. In addition, resultant wear scar profiles of each material measured after 10N and 30N wear testing can be seen in Fig. 10.

PTFE-PA12 was the only solid lubricant filled composite that was less resistant to wear than neat-PA12. As can be seen in Fig. 8b, this was exacerbated when normal loads were increased from 10N to 30N which resulted in an increase in specific wear rate from 11.7% to 43.0% relative to neat-PA12, respectively. These adverse wear rates were primarily due to PTFE-PA12 being softer and more ductile than neat-PA12. As previously discussed in Section 3.3, PTFE-PA12 was 77.8% more ductile than neat-PA12, this coupled with virgin PTFE having a Shore D hardness of 60 [62] compared to 75 for PA12 [40], will have resulted in PTFE-PA12 being more susceptible to abrasive wear, specifically ploughing.

Furthermore, it can be seen in Fig. 9 that material transfer to the pin counterface was most abundant during the 10N wear testing of PTFE-PA12. However, when the applied load was increased to 30N the mechanism of material transfer for PTFE-PA12 was alike every other

**Table 5**
Mean coefficient of friction and specific wear rates for each material tested, as well as their corresponding standard deviations.

| Material | Coefficient of friction | | Specific wear rate ($10^{-4}$ $mm^3$/Nm) | |
|---|---|---|---|---|
| | 10N | 30N | 10N | 30N |
| PA12 | 0.305 (± 0.010) | 0.261 (± 0.011) | 4.782 (± 0.086) | 3.197 (± 0.147) |
| PTFE-PA12 | 0.192 (± 0.011) | 0.128 (± 0.005) [a] | 5.343 (± 0.082) | 4.480 (± 0.141) |
| Graphite-PA12 | 0.289 (± 0.009) | 0.246 (± 0.012) | 2.782 (± 0.056) | 1.139 (± 0.070) |
| $MoS_2$-PA12 | 0.304 (± 0.005) | 0.257 [b] | 1.033 (± 0.116) | 1.465 [b] |

[a] Mean coefficient of friction value was computed prior to the breakdown in lubrication.
[b] Due to curl only a single 30N wear test could be performed for $MoS_2$-PA12 samples.

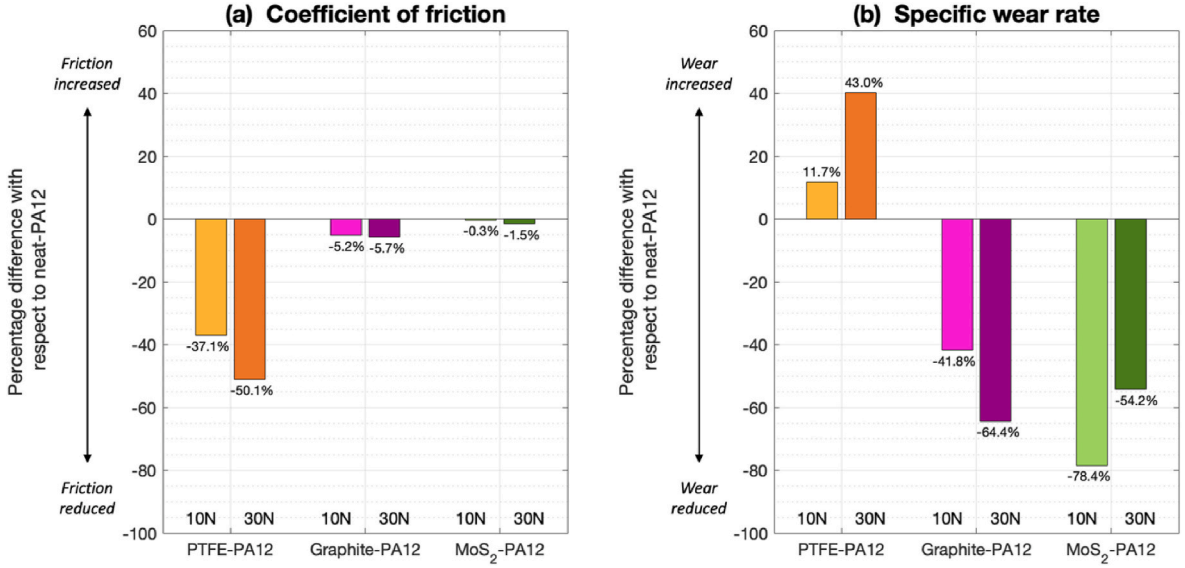


**Fig. 8.** Percentage difference in resultant (a) coefficient of friction and (b) specific wear rate values of solid lubricant filled polymeric composites with respect to neat-PA12 samples.

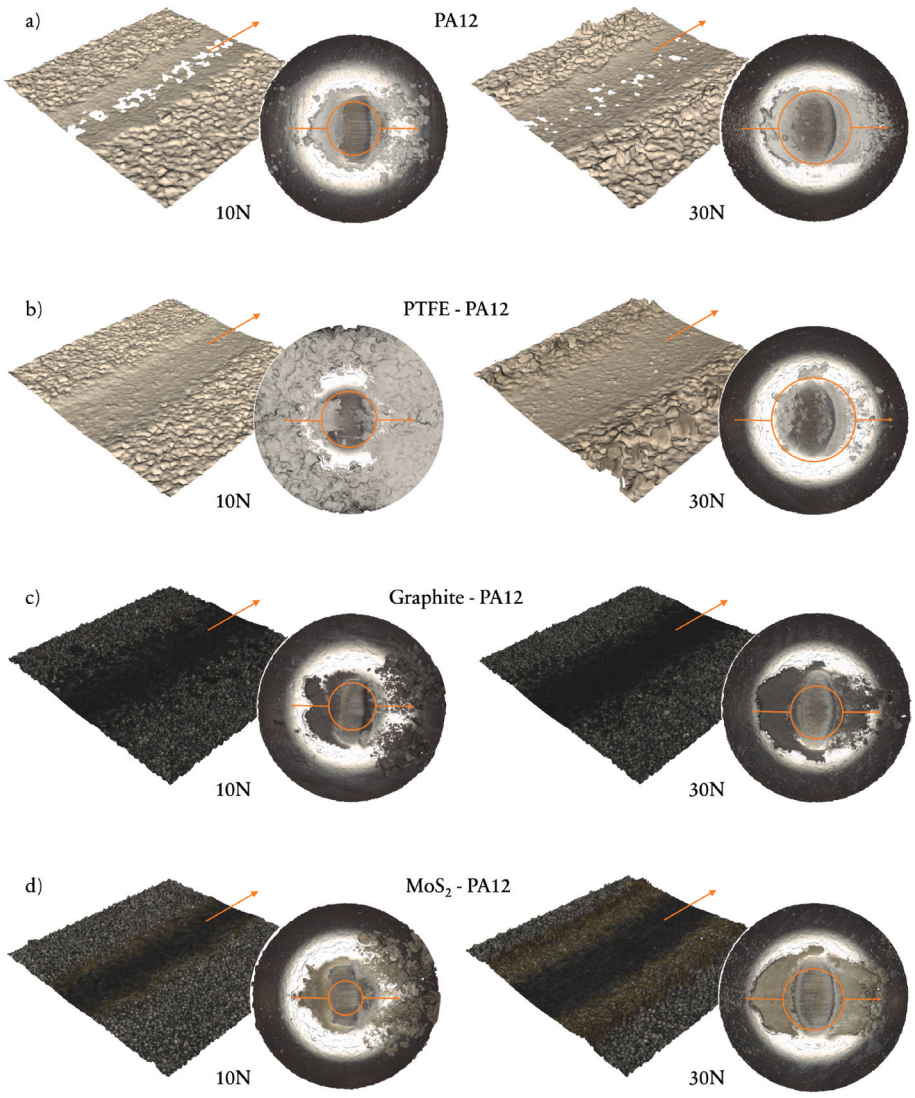


**Fig. 9.** Resultant (a) PA12, (b) PTFE-PA12, (c) Graphite-PA12 and (d) $MoS_2$-PA12 surfaces and corresponding pin counterfaces after 10N and 30N wear testing. Sliding directions and contact areas are given by solid orange annotations. The missing information in the PA12 wear scars was due to its worn surfaces being highly reflective which inhibited light from being received by the microscope's detector. (For interpretation of the references to colour in this figure legend, the reader is referred to the Web version of this article.)

material tested in this study independent of applied load. In Fig. 9 it can be seen that resultant wear debris adhered tentatively to the leading edge of the pin, but more securely at the rear. More specifically, the latter was characteristic of adhesive wear, whereby frictional heating induced thermal softening resulted in the visibly thick and coalesced wear debris adhering to the rear edge of each counterface.

The addition of Graphite and $MoS_2$ within PA12 significantly reduced resultant composite specific wear rates relative to neat-PA12. At lower loads, $MoS_2$-PA12 exhibited the greatest resistance to wear. Furthermore, discolouration at the edges of the $MoS_2$-PA12 wear scar visible in Fig. 9d suggests that the solid lubricant accumulated at the wear track boundary and was active in supporting both the10 N and 30N applied normal loads. Whereas at higher loads, Graphite-PA12 was the most effective solid lubricant filled composite at reducing wear. More specifically, the inclusion of Graphite reduced specific wear rate by 64.4% on average relative to neat-PA12 during 30N wear testing.

In addition, Fig. 10 shows the vertical height deviations within Graphite-PA12 and $MoS_2$-PA12 wear scars to be comparatively smaller than that of neat-PA12 and PTFE-PA12 independent of applied load. Graphite-PA12 and $MoS_2$-PA12 surfaces were therefore more resistant to abrasive scratching that incurred from the harder asperities on each corresponding counterface during wear testing. Singh et al. [63] demonstrated that the indentation hardness of Laser Sintered PA12 surfaces is positively correlated to their powder bed temperatures during building, in this study the latter was found to increase as result of Graphite and $MoS_2$ as discussed in Section 3.1.

## 4. Conclusions

The present work investigated solid lubricant inclusion within Laser Sintered PA12, specifically whether the addition of PTFE, Graphite and $MoS_2$ influenced LS processability, as well as resultant mechanical and tribological performance.

SEM analysis showed that homogenous composite powder blends were attainable via simple mixing methods, without any negative effect on powder flow. However, during Laser Sintering curl occurred in Graphite-PA12 and $MoS_2$-PA12 samples due to their powder beds being more thermally conductive, and thus differential shrinkage was induced at their part edges. Despite this, resultant top surface topographies of all composites were in good agreement with neat-PA12. Furthermore, tensile testing highlighted that solid lubricant inclusion did not compromise resultant composite mechanical performance.

An inverse trend between friction and wear was observed when comparing the tribological performance of solid lubricant reinforced PA12 composites, independent of load. PTFE-PA12 experienced the most wear, despite sliding with the least resistance, whereas Graphite-PA12 and $MoS_2$-PA12 had the smallest mean specific wear rates, even though they incurred the greatest friction. Wear resistance was also

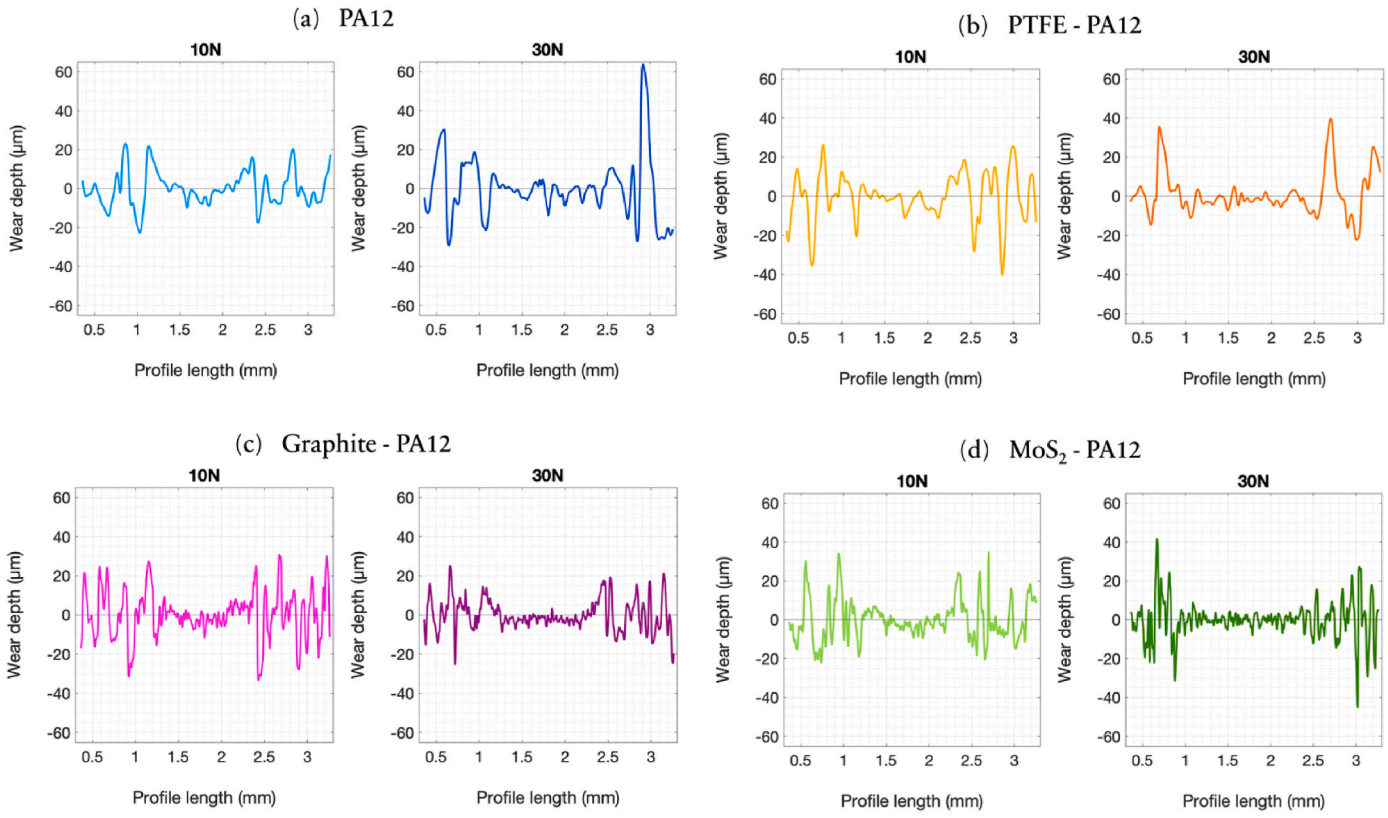


**Fig. 10.** Resultant (a) PA12, (b) PTFE-PA12, (c) Graphite-PA12 and (d) $MoS_2$-PA12 wear scar profiles evaluated by FV microscopy.

correlated with the resultant tensile properties of parts produced. Moreover, it was demonstrated that the individual inclusions of PTFE and $MoS_2$ could reduce the coefficient of friction and specific wear rate of Laser Sintered PA12 components by as much as 50.1% and 78.4%, respectively.

This research serves as a benchmark for future studies that will focus on optimising the friction and wear properties of Laser Sintered PA12 components by solid lubricant addition.

## Funding

The authors would like to acknowledge the support of the EPSRC Future Manufacturing Hub in Manufacture Using Advanced Powder Processes (EP/P006566/1), as well as the EPSRC (DTP account EP/N509735/1) for partially funding the PhD studentship this research is based on. For the purpose of open access, the author has applied a Creative Commons Attribution (CC BY) licence to any Author Accepted Manuscript version arising.

## Declaration of competing interest

The authors declare that they have no known competing financial interests or personal relationships that could have appeared to influence the work reported in this paper.

## Acknowledgements

The author would like to thank Wendy Birtwistle for her kind assistance during Laser Sintering.

## References

[1] F. Sillani, R. Schiegg, M. Schmid, E. Macdonald, K. Wegener, Powder surface roughness as proxy for bed density in powder bed fusion of polymers, Polymers 14 (2022) 1–10, https://doi.org/10.3390/polym14010081.
[2] T. Wohlers, I. Campbell, O. Diegel, J. Kowen, N. Mostow, Wohlers Report 2022: 3D Printing and Additive Manufacturing, Global State of the Industry, Washington DC, 2022.
[3] A. Averardi, C. Cola, S.E. Zeltmann, N. Gupta, Effect of particle size distribution on the packing of powder beds: a critical discussion relevant to additive manufacturing, Mater. Today Commun. 24 (2020), https://doi.org/10.1016/j.mtcomm.2020.100964.
[4] Y. Wang, Z. Xu, D. Wu, J. Bai, Current status and prospects of polymer powder 3D printing technologies, Materials 13 (2020), https://doi.org/10.3390/ma13102406.
[5] ASTM International, ASTM F2792-12a - Standard Terminology for Additive Manufacturing Technologies, 2013, pp. 10–12, https://doi.org/10.1520/F2792-12A.2.
[6] S. Petzold, J. Klett, T.A. Osswald, A statistical study of surface roughness for polyamide 12 parts produced using selective laser sintering, Int. Polym. Process. 35 (2020) 126–138, https://doi.org/10.3139/217.3900.
[7] J. Kruth, G. Levy, R. Schindel, T. Craeghs, E. Yasa, Consolidation of polymer powders by selective laser sintering, in: 3rd Int. Conf. Polym. Mould. Innov., 2008. Ghent, Belgium.
[8] P. Chen, M. Tang, W. Zhu, L. Yang, S. Wen, C. Yan, Z. Ji, H. Nan, Y. Shi, Systematical mechanism of Polyamide-12 aging and its micro-structural evolution during laser sintering, Polym. Test. 67 (2018) 370–379, https://doi.org/10.1016/j.polymertesting.2018.03.035.
[9] L.J. Tan, W. Zhu, K. Zhou, Recent progress on polymer materials for additive manufacturing, Adv. Funct. Mater. (2020) 1–54, https://doi.org/10.1002/adfm.202003062, 2003062.
[10] M. Schmid, A. Amado, K. Wegener, Polymer powders for selective laser sintering (SLS), AIP Conf. Proc. 1664 (2015), https://doi.org/10.1063/1.4918516.
[11] B. Yao, Z. Li, F. Zhu, Effect of powder recycling on anisotropic tensile properties of selective laser sintered PA2200 polyamide, Eur. Polym. J. 141 (2020), 110093, https://doi.org/10.1016/j.eurpolymj.2020.110093.
[12] N. Ma, W. Liu, L. Ma, S. He, H. Liu, Z. Zhang, A. Sun, M. Huang, C. Zhu, Crystal transition and thermal behavior of Nylon 12, E-Polymers 20 (2020) 346–352, https://doi.org/10.1515/epoly-2020-0039.
[13] D. Rouholamin, N. Hopkinson, Understanding the Efficacy of Micro-CT to Analyse High Speed Sintering Parts, vol. 1, 2016, pp. 152–161, https://doi.org/10.1108/RPJ-03-2014-0030.
[14] J. Bijwe, V. Naidu, N. Bhatnagar, M. Fahim, Optimum concentration of reinforcement and solid lubricant in polyamide 12 composites for best tribo-

performance in two wear modes, Tribol. Lett. 21 (2006) 57–64, https://doi.org/10.1007/s11249-005-9010-7.
[15] S. Yuan, F. Shen, C.K. Chua, K. Zhou, Polymeric composites for powder-based additive manufacturing: materials and applications, Prog. Polym. Sci. 91 (2019) 141–168, https://doi.org/10.1016/j.progpolymsci.2018.11.001.
[16] C. Yan, L. Hao, L. Xu, Y. Shi, Preparation, characterisation and processing of carbon fibre/polyamide-12 composites for selective laser sintering, Compos. Sci. Technol. 71 (2011) 1834–1841, https://doi.org/10.1016/j.compscitech.2011.08.013.
[17] A. Mousah, Effects of Filler Content and Coupling Agents on the Mechanical Properties and Geometrical Accuracy of Selective Laser Sintered Parts in Glass Bead-Filled Polyamide 12 Composites, Cardiff University, 2011. http://orca.cf.ac.uk/11094/.
[18] R.D. Goodridge, C.J. Tuck, R.J.M. Hague, Laser sintering of polyamides and other polymers, Prog. Mater. Sci. 57 (2012) 229–267, https://doi.org/10.1016/j.pmatsci.2011.04.001.
[19] H. Chung, S. Das, Functionally graded Nylon-11/silica nanocomposites produced by selective laser sintering, Mater. Sci. Eng. 487 (2008) 251–257, https://doi.org/10.1016/j.msea.2007.10.082.
[20] S. Yuan, F. Shen, C.K. Chua, K. Zhou, Polymeric composites for powder-based additive manufacturing: materials and applications, Prog. Polym. Sci. 91 (2019) 141–168, https://doi.org/10.1016/j.progpolymsci.2018.11.001.
[21] C.E. Majewski, H. Zarringhalam, D. Toon, U. Ajoku, N. Hopkinson, M.P. Caine, The use of off-line part production to predict the tensile properties of parts produced by Selective Laser Sintering, J. Mater. Process. Technol. 209 (2009) 2855–2863, https://doi.org/10.1016/j.jmatprotec.2008.06.037.
[22] Y. Liu, L. Zhu, L. Zhou, Y. Li, Microstructure and mechanical properties of reinforced polyamide 12 composites prepared by laser additive manufacturing, Rapid Prototyp. J. 25 (2019) 1127–1134, https://doi.org/10.1108/RPJ-08-2018-0220.
[23] A. Mazzoli, G. Moriconi, M.G. Pauri, Characterization of an aluminum-filled polyamide powder for applications in selective laser sintering, Mater. Des. 28 (2007) 993–1000, https://doi.org/10.1016/j.matdes.2005.11.021.
[24] J. Yang, Y. Shi, C. Yan, Selective laser sintering of polyamide 12/potassium titanium whisker composites, J. Appl. Polym. Sci. 117 (2010) 2196–2204, https://doi.org/10.1002/app.31965.
[25] J. Bai, J. Song, J. Wei, Tribological and mechanical properties of MoS2 enhanced polyamide 12 for selective laser sintering, J. Mater. Process. Technol. 264 (2019) 382–388, https://doi.org/10.1016/j.jmatprotec.2018.09.026.
[26] M. Batistella, A. Regazzi, M.F. Pucci, J.M. Lopez-Cuesta, O. Kadri, D. Bordeaux, F. Ayme, Selective laser sintering of polyamide 12/flame retardant compositions, Polym. Degrad. Stabil. 181 (2020), 109318, https://doi.org/10.1016/j.polymdegradstab.2020.109318.
[27] R.D. Turner, J.R. Wingham, T.E. Paterson, J. Shepherd, C. Majewski, Use of silver-based additives for the development of antibacterial functionality in Laser Sintered polyamide 12 parts, Sci. Rep. 10 (2020) 1–11, https://doi.org/10.1038/s41598-020-57686-4.
[28] Y. Chunze, S. Yusheng, Y. Jinsong, L. Jinhui, A nanosilica/nylon-12 composite powder for selective laser sintering, J. Reinforc. Plast. Compos. 28 (2009) 2889–2902, https://doi.org/10.1177/0731684408094062.
[29] J. Bai, R.D. Goodridge, R.J.M. Hague, M. Song, Improving the mechanical properties of laser-sintered polyamide 12 through incorporation of carbon nanotubes, Polym. Eng. Sci. 53 (2013) 1937–1946, https://doi.org/10.1002/pen.23459.
[30] K. Friedrich, Z. Zhang, A.K. Schlarb, Effects of various fillers on the sliding wear of polymer composites, Compos. Sci. Technol. 65 (2005) 2329–2343, https://doi.org/10.1016/j.compscitech.2005.05.028.
[31] T.W. Scharf, S.V. Prasad, Solid lubricants: a review, J. Mater. Sci. 48 (2013) 511–531, https://doi.org/10.1007/s10853-012-7038-2.
[32] J.C.J. Bart, E. Gucciardi, S. Cavallaro, Lubricants: Properties and Characteristics, Biolubricants, 2013, pp. 24–73, https://doi.org/10.1533/9780857096326.24.
[33] G. Mariani, Selection and application of solid lubricants as friction modifiers, in: Lubr. Addit. Chem. Appl., Third, 2015, p. 249, https://doi.org/10.1201/b19209-17, 249.
[34] J. Ye, H.S. Khare, D.L. Burris, Quantitative characterization of solid lubricant transfer film quality, Wear 316 (2014) 133–143, https://doi.org/10.1016/j.wear.2014.04.017.
[35] R. Kumar, H. Kumar Banga, H. Singh, S. Kundal, An outline on modern day applications of solid lubricants, Mater. Today Proc. 28 (2020) 1962–1967, https://doi.org/10.1016/j.matpr.2020.05.558.
[36] B. Ben Difallah, M. Kharrat, M. Dammak, G. Monteil, Mechanical and tribological response of ABS polymer matrix filled with graphite powder, Mater. Des. 34 (2012) 782–787, https://doi.org/10.1016/j.matdes.2011.07.001.
[37] K. Bashandeh, P. Lan, J.L. Meyer, A.A. Polycarpou, Tribological performance of graphene and PTFE solid lubricants for polymer coatings at elevated temperatures, Tribol. Lett. 67 (2019) 1–14, https://doi.org/10.1007/s11249-019-1212-5.
[38] S. Bahadur, D. Tabor, The wear of filled polytetrafluoroethylene, Wear 98 (1984) 1–13, https://doi.org/10.1016/0043-1648(84)90213-8.
[39] D.X. Li, Y.L. You, X. Deng, W.J. Li, Y. Xie, Tribological properties of solid lubricants filled glass fiber reinforced polyamide 6 composites, Mater. Des. 46 (2013) 809–815, https://doi.org/10.1016/j.matdes.2012.11.011.
[40] EOS GmbH - Electro Optical Systems, PA2200 Material Data Sheet, 2017.
[41] BSI-Standards, BS EN ISO 25178-2:2012 - Geometrical Product Specifications (GPS). Surface Texture: Areal. Part 2: Terms, Definitions and Surface Texture Parameters, 2022, p. 74.
[42] S. Petzold, J. Klett, A. Schauer, T.A. Osswald, Surface roughness of polyamide 12 parts manufactured using selective laser sintering, Polym. Test. 80 (2019), 106094, https://doi.org/10.1016/j.polymertesting.2019.106094.
[43] L. Newton, N. Senin, C. Gomez, R. Danzl, F. Helmli, L. Blunt, R. Leach, Areal topography measurement of metal additive surfaces using focus variation microscopy, Addit. Manuf. 25 (2019) 365–389, https://doi.org/10.1016/j.addma.2018.11.013.
[44] Z. Zhu, S. Lou, C. Majewski, Characterisation and correlation of areal surface texture with processing parameters and porosity of High Speed Sintered parts, Addit. Manuf. 36 (2020), https://doi.org/10.1016/j.addma.2020.101402.
[45] BSI-Standards, BS EN ISO 13565-1:1998 - Geometric Product Specifications (GPS). Surface Texture: Profile Method. Surfaces Having Stratified Functional Properties. Part 1: Filtering and General Measurement Conditions, 1998, p. 16.
[46] ASTM International, D638−14 - Standard Test Method for Tensile Properties of Plastics, 2015, pp. 1–16, https://doi.org/10.1520/D0638-14.1.
[47] Standard Test Method for Wear Testing with a Pin-on-Disk Apparatus, ASTM Stand. G99. (2017) 1-6. https://doi.org/10.1520/G0099-17.Copyright.
[48] S.P. Soe, Quantitative analysis on SLS part curling using EOS P700 machine, J. Mater. Process. Technol. 212 (2012) 2433–2442, https://doi.org/10.1016/j.jmatprotec.2012.06.012.
[49] M. Yuan, T.T. Diller, D. Bourell, J. Beaman, Thermal conductivity of polyamide 12 powder for use in laser sintering, Rapid Prototyp. J. 19 (2013) 437–445, https://doi.org/10.1108/RPJ-11-2011-0123.
[50] A.N. Gandi, U. Schwingenschlögl, Thermal conductivity of bulk and monolayer MoS2, EPL 113 (2016), https://doi.org/10.1209/0295-5075/113/36002.
[51] H. Tu, L. Ye, Thermal conductive PS/graphite composites, Polym. Adv. Technol. 20 (2009) 21–27, https://doi.org/10.1002/pat.1236.
[52] R.D. Goodridge, R.J.M. Hague, C.J. Tuck, An empirical study into laser sintering of ultra-high molecular weight polyethylene (UHMWPE), J. Mater. Process. Technol. 210 (2010) 72–80, https://doi.org/10.1016/j.jmatprotec.2009.08.016.
[53] D.L. Bourell, T.J. Watt, D.K. Leigh, B. Fulcher, Performance limitations in polymer laser sintering, Phys. Procedia 56 (2014) 147–156, https://doi.org/10.1016/j.phpro.2014.08.157.
[54] M. Vetterli, M. Schmid, K. Wegener, Comprehensive Investigation of Surface Characterization Methods for Laser Sintered Parts, 2018.
[55] K. Nar, C. Majewski, R. Lewis, A comprehensive characterisation of Laser Sintered Polyamide-12 surfaces, Polym. Test. 106 (2021), 107450, https://doi.org/10.1016/j.polymertesting.2021.107450.
[56] A.E. Tontowi, T.H.C. Childs, Density prediction of crystalline polymer sintered parts at various powder bed temperatures, Rapid Prototyp. J. 7 (2001) 180–184, https://doi.org/10.1108/13552540110395637.
[57] T. Kigure, Y. Yamauchi, T. Niino, Relationship between powder bed temperature and microstructure of laser sintered PA12 parts, in: Solid Free. Fabr. 2019 Proc. 30th Annu. Int. Solid Free. Fabr. Symp. - an Addit. Manuf. Conf. SFF 2019, 2019, pp. 827–834.
[58] X. Lua, Y. Jin, Structure and properties of Nylon 12/SiC nanocomposites, Mater. Res. Express 6 (2019), https://doi.org/10.1088/2053-1591/ab0874.
[59] W. Brostow, D. Zhang, Tensile elongation at break for polymers related to Vickers hardness, Mater. Lett. 276 (2020), 128179, https://doi.org/10.1016/j.matlet.2020.128179.
[60] S. Sathees Kumar, G. Kanagaraj, Investigation on mechanical and tribological behaviors of PA6 and graphite-reinforced PA6 polymer composites, Arabian J. Sci. Eng. 41 (2016) 4347–4357, https://doi.org/10.1007/s13369-016-2126-2.
[61] J. Guo, J. Bai, K. Liu, J. Wei, Surface quality improvement of selective laser sintered polyamide 12 by precision grinding and magnetic field-assisted finishing, Mater. Des. 138 (2017) 39–45, https://doi.org/10.1016/j.matdes.2017.10.048.
[62] P.M.F. Wani, Tribological behaviour of virgin Ptfe and glass filled Ptfe under dry sliding conditions, in: Innov. Approaches Mech. Eng., n.d.: pp. 5–11.
[63] S. Singh, A. Sachdeva, V.S. Sharma, Optimization of selective laser sintering process parameters to achieve the maximum density and hardness in polyamide parts, Prog. Addit. Manuf. 2 (2017) 19–30, https://doi.org/10.1007/s40964-017-0020-4.